Generic Epitaxial Graphene Biosensors for Ultrasensitive Detection of Cancer Risk Biomarker

Z. Tehrani[1], G.Burwell[1], M.A.Mohd Azmi[1],A.Castaing[1], R.Rickman[2], J. Almarashi[2], P.Dunstan[2], A. Miran Beigi[3], S.H. Doak[4] and O.J. Guy[1*]*

[1] College of Engineering, Swansea University, Singleton Park, Swansea, UK
[2] College of Science, Swansea University, Singleton Park, Swansea, UK
[3]Research Institute of Petroleum Industry, Tehran, Iran
[4]College of Medicine, Swansea University, Singleton Park, Swansea, UK
[1*]Corresponding authors: E-mail address:
Z.Tehrani@swansea.ac.uk and O.J.Guy@swansea.ac.uk

Abstract

A generic electrochemical method of "bioreceptor" antibody attachment to phenyl amine functionalised graphitic surfaces is demonstrated. Micro-channels of chemically modified multi-layer epitaxial graphene (MLEG) have been used to provide a repeatable and reliable response to nano molar (nM) concentrations of the cancer risk (oxidative stress) biomarker 8-hydroxydeoxyguanosine (8-OHdG). X-ray photoelectron spectroscopy, Raman spectroscopy are used to characterize the functionalised MLEG. Confocal fluorescence microscopy using fluorescent-labelled antibodies indicates that the anti-8-OHdG antibody selectively binds to the phenyl amine-functionalised MLEG's channel. Current-voltage measurements on functionalised channels showed repeatable current responses from antibody-biomarker binding events. This technique is scalable, reliable, and capable of providing a rapid, quantitative, label-free assessment of biomarkers at nano-Molar (less than 20 nM) concentrations in analyte solutions. The sensitivity of the sensor device was investigated using varying concentrations of 8-OHdG, with changes in the sensor's channel resistance observed upon exposure to 8-OHdG. Detection of 8-OHdG concentrations as low as 0.1ng/ml

[1] Corresponding authors. Tel.+44 (0) 1792-295532 E-mail: Z.Tehrani@swansea.ac.uk
Tel.+44 (0) 1792-513181 E-mail: O.J.Guy@swansea.ac.uk

(0.35 nM) has been demonstrated. This is five times more sensitive than reported Enzyme Linked Immunosorbent Assay tests (0.5 ng/ml).

1. Introduction

The exceptional electronic and thermal properties of graphene are particularly suitable for a range of new applications from flexible electronics to functional nanodevices [1, 2], such as biosensors [3], gas sensors [4] and high performance transistors [5-8].

Graphene devices and sensors promise to be a disruptive technology in next generation electronics and healthcare diagnostic applications - due to graphene's exceptional electronic properties and extreme surface to volume ratio which offer greatly enhanced sensitivity. Graphene devices also provide the potential for portable rapid diagnostic point-of-care (POC) sensors - compared to conventional labour intensive, time consuming enzyme-linked immunobsorbant assays (ELISAs) that are currently used for clinical biomarker analysis.

For graphene sensors to be viable, consistent quality, large area graphene must be sourced. The main issue with exfoliated graphene is the lack of a production method for large area graphene. In contrast, epitaxial graphene can be grown on large area semi-insulating silicon carbide (SiC) substrates and is an amenable form of graphene for electronics and sensors, as devices can be fabricated on large area graphene using standard semiconductor wafer processing techniques and without the need for any layer transfer [8, 9].

The surface chemistry of graphene can be modified in a similar manner to that of Highly Ordered Pyrolytic Graphite (HOPG), glassy carbon, or Carbon Nanotubes (CNT) [10, 11]. Diazonium salts are widely used to functionalise carbon nanotubes [12] and graphene[13-15], forming a covalent bond between the CNT / graphene and an aryl group. The aryl diazonium cation accepts an electron from the substrate and generates an aryl radical by releasing a nitrogen molecule. This covalent modification strategy has recently been applied to both epitaxial graphene on SiC [16], chemically converted graphene (CCG) [17] and mechanically exfoliated graphene [18].

Chemical functionalisation of graphene can be used to tailor the chemical specificity and the electronic properties of graphene *via* doping and band-gap engineering [15, 19-24].

The use of exfoliated graphene as a biosensor has been previously demonstrated in the detection of analytes, including hydrogen peroxide, glucose oxidase, and DNA [25].

In this article, we present an electrochemical method for functionalisation of ultra-sensitive graphene biosensors, fabricated using epitaxial graphene on silicon carbide. This is the first report of an epitaxial graphene channel biosensor for detection of a cancer risk biomarker.

Epitaxial graphene grown on the carbon face of 4H-SiC has been characterised using XPS and Raman spectroscopy. Graphene channel devices, fabricated using electron beam lithography, have been used as the basis for graphene sensors.

Generic functionalisation technology, using a versatile phenyl amine linking group has been used to graft a "bioreceptor" antibody, targeted against the oxidative stress marker 8-OHdG, to the epitaxial graphene channel (Figure 1).

Bioreceptor molecules are attached to graphene *via* a phenyl amine group ($PhNH_2$), introduced by reduction of a nitro-phenyl group ($PhNO_2$) [12, 15, 26, 27].
Monoclonal antibody bioreceptors, targeted against the oxidative stress-induced DNA adduct 8-hydroxydeoxyguanosine (8-OHdG), have been attached to the amino functionalised graphene in prototype biosensors.

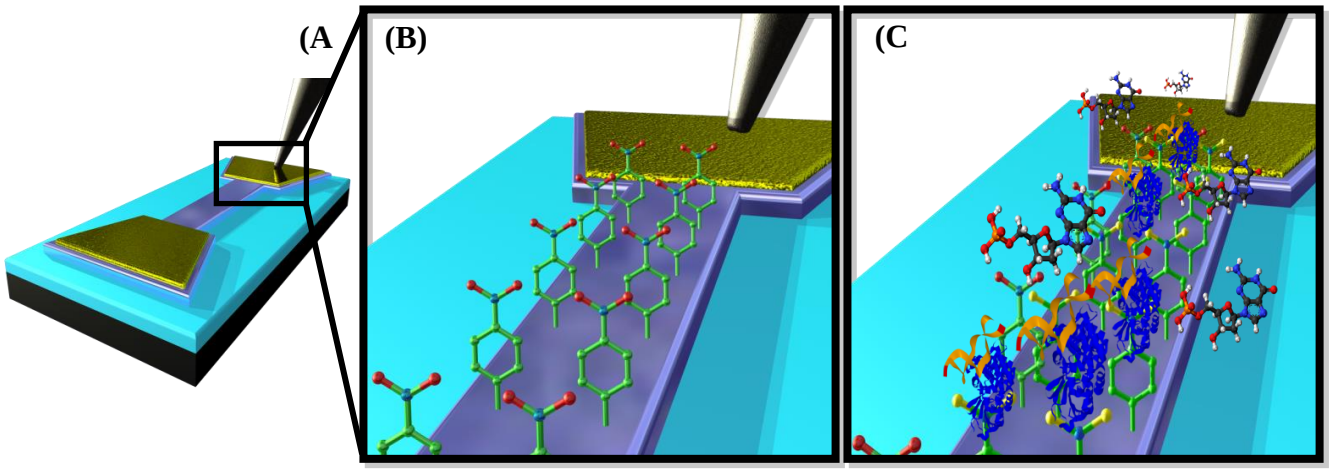

Figure 1: Illustration of an epitaxial graphene channel biosensor for detection of targeted 8-hydroxydeoxyguanosine (8-OHdG) biomarker. (A) Schematic of MLEG device (B) Thin film of covalently attached nitro phenyl ($PhNO_2$) groups on the MLEG channel. (C) Attachment of the "bioreceptor" antibody anti-8-OHdG to the amine terminated MLEG channel and subsequent detection of 8-OHdG.

The antibody functionalised graphene is capable of selective binding to the 8-OHdG biomarker [28-30].
The presence of 8-OHdG in blood, urine and saliva, is commonly associated with DNA damage induced through an oxidative stress related mechanism, and has been identified as a risk factor for the development of cancer. Elevated levels of 8-OHdG have been linked to

increased risk of developing several cancers [28-30] and 8-OHdG detection has been used to successfully differentiate patients with bladder and prostate cancer from healthy patients [31, 32].

However, 8-OHdG is typically present at very low concentrations in urine (nM) and limited sensitivity ELISAs are inadequate for early stage detection of the disease biomarker [33]. A prototype biosensor for detection of 8-OHdG using highly sensitive, label-free, electrochemical graphene nano-biochips is thus an important development in early stage detection of cancer risk.

2. Experimental

2.1. Materials and reagents

4H-SiC, C-terminated, on-axis, semi-insulating substrates were purchased from Cree, Inc. Poly methyl methacrylate (PMMA), photoresist ECI 3027 and developer AZ 726 MF, were purchased from Micro Chem. 4-nitrobenzene diazonium tetrafluoroborate (4-NPD) and tetrabutylammonium tetrafluoroborate (NBu_4BF_4) electrolyte, bovine serum albumin (BSA), phosphate buffered saline (PBS), were all purchased from Sigma-Aldrich. Acetonitrile (CH_3CN), dichloromethane (CH_2Cl_2) and acetone, supplied by Fisher, were used to clean the graphene of physisorbed organic residues after the chemical functionalisation reaction.

The 3-electrodes used, aqueous references electrode (Ag/AgCl) and non-aqueous references electrode (Ag/Ag^+) were purchased from IJ Cambria Scientific Ltd and the third platinum (Pt) electrode was purchased from BASi Analytical Instruments. Anti-8-OHdG antibody was purchased from Abcam (UK). Target 8-OHdG was supplied by the Cayman Chemical Company.

2.2. Apparatus

Graphene growth was performed in a Jipelec rapid thermal processing SiC furnace fitted with a turbo molecular pump. An e-Line (Raith GmBH) electron beam lithography system was used to define the graphene channels and contacts of the sensor device. Plasma etching of the graphene device was performed in an Oxford Instruments PlasmaLab 80 plus and metal deposition was performed using a Kurt J. Lesker PVD 75 sputtering system.

Cyclic voltammetry measurements were performed using an EmStat2 Palm Sens potentiostat with the graphene channel device as the working electrode, a Pt auxiliary electrode and

Ag/AgCl reference electrode. Electrical measurements were performed using a Semi Probe LA-150 probe station with a Keithley 2602A Source Meter. Micro-Raman measurements were performed using a Renishaw InVia system with a 100 mW, 532 nm excitation laser with approximately 10 mW of power on the sample. X-ray photoelectron spectroscopy (XPS) measurements were performed in a VG ESCAlab MKII with an Al X-ray excitation source (Kα of 1486 eV).

In this work a laser scanning confocal Fluorescence microscope (Carl Zeiss LSM 710) was used to detect fluorescence from bio-functionalised channel and verify successful antibody attachment to the epitaxial graphene channel via fluorescent emission from a conjugated secondary antibody. The excitation and emission wavelength of the Q-dot labelled secondary antibody (supplied by Abcam) were 530 nm and 651– 658 nm respectively.

2.3. Fabrication of epitaxial graphene biosensor array

Epitaxial graphene has been grown *via* silicon sublimation on the carbon face of 4H silicon carbide (4H-SiC), by annealing at high temperature (1750°C) and at and low pressure (1×10^{-4} mbar).

Following graphene growth on 10 mm by 10mm SiC samples, were spin coated with Poly methyl methacrylate (PMMA).

PMMA in chlorobenzene (in a 1:3 wt ratio), photoresist ECI 3027 and developer AZ 726 MF, were used for lithographic patterning of the graphene channel devices. Sensor arrays, using micro-channel graphene sensing elements between two metal electrodes, were fabricated on epitaxial graphene using electron beam lithography (EBL) with channel width 250 μm and the channel length 3mm.

Following development of the resist, 50 nm of aluminium was sputtered onto the graphene, and then selectively removed using warm acetone in a lift-off process. Exposed graphene was then etched using oxygen plasma for 30 seconds at 50 W, 50 sccm O_2, 75 mTorr.

The aluminium mask was removed using concentrated hydrofluoric acid (HF), leaving patterned graphene on the SiC surface. Physical Vapour Deposition (PVD) of Ti/Au: 100 nm/ 200 nm followed by electron beam lithography patterning and subsequent lift-off in warm acetone was used to fabricate the metal source and drain contacts at either end of the graphene channel.

2.4. Surface Functionalisation via diazotization

The graphene channel devices were modified via diazotization reaction. Graphene samples were subsequently immersed into a solution of 2mM (4-NPD) and 0.1 M (Bu_4NBF_4) in acetonitrile. The electrochemical reaction between graphene and 4-NPD was performed with a conventional three-electrode cell, which included an Ag/Ag^+ reference electrode, a platinum wire counter electrode, and the epitaxial graphene channel working electrode, at room temperature for duration of 5-15 minutes. Cyclic voltammograms (CVs) were carried out at a scan rate of 100 mV s^{-1} in a 0.1 M (Bu_4NBF_4) in acetonitrile. Following completion of the reaction, indicated by cyclic voltammetry, the samples were rinsed in acetonitrile followed by CH_2Cl_2, in order to remove any residual chemical reagents. Finally, the samples were washed with acetone and dried under a flow of N_2.

After attachment of nitro- phenyl groups to the graphene surface, reduction of the nitro-group to phenyl amine was performed in 0.1M KCl water / Ethanol (9:1) solution, using chronoamperometry. A constant voltage of -0.9V was applied between the Ag/ AgCl and the graphene-working electrode for 100 seconds until a stable current was achieved. This indicates that the reduction reaction is near completion.

This newly reported chronoamperometric reduction process has several advantages compared to previously reported diazotisations [12, 15, 26, 27]. It takes a far shorter time (just a few minutes) compared to several hours (16); it does not need to be performed in a dark environment and purging argon or nitrogen gas for the exclusion of oxygen is not required [34, 35].

This paper reports this rapid electrochemical functionalisation process for the first time on epitaxial graphene[36]. The advantage of this functionalisation method lies in its simplicity, avoidance of harsh oxidation chemistry and speed of reaction.

2.5. Biofunctionalisation

Following phenyl amine functionalisation of graphene, antibodies targeted against 8-OHdG must be attached to the graphene.

The primary antibody, mouse monoclonal anti-8 Hydroxyguanosine (anti-8OHdG, purchased from Abcam, UK), was diluted in phosphate buffered saline (PBS) pH 7.4 to a concentration of 2 μg/ml. Diluted primary antibody was applied to the graphene channels and incubated at 4°C for 4 hours before rinsing 4 times in double deionised (DI) water and subsequent drying.

To confirm successful and specific binding of the primary antibody to the graphene channel, a fluorescently labelled secondary antibody was subsequently applied to the functionalised graphene channel. The fluorescent label used was a quantum-dot functionalised secondary antibody (goat F(ab`)2 anti-mouse IgG conjugate (H+L), labelled with Qdot 655). This secondary antibody was applied to the graphene channel for three hours, at 4°C then rinsed with deionised water prior to fluorescent microscopy.

In order to prevent nonspecific binding of proteins in the fluorescent detection step, any remaining free amine groups that had not react with the primary antibody on the sensor surface were passivated using 5% bovine serum albumin (BSA) in PBS for 10 minutes at room temperature. Substrates were subsequently rinsed 3 times in DI water and dried. The secondary antibody, Qdot 655 goat F(ab')2 anti-mouse IgG conjugate (Life Technologies Ltd, UK), was diluted to 20 nM in PBS pH 7.4 and applied to the graphene channels. Excess unbound secondary antibodies were removed by rinsing 5 times in double DI water.

2.6. Electrical characteristics

Characterisation of epitaxial graphene channel device was performed using a Hewlett Packard 4142B DC parametric analyser running ITC Characterisation software in conjunction with a probe station.

Current–voltage (I–V) measurements were performed using a voltage sweep of -1V to +1 V between the two metal contacts of the epitaxial graphene channel. Electrical detection of functionalisation and biomarker binding of graphene has been monitored at each stage of the functionalisation process.

3. Results and discussion

3.1 Characterization of graphene devices

The high surface-to-volume ratio of these graphene channels contributes to their high sensitivity to their surface chemical environment [37].

Graphene growth can be controlled to produce a graphene layer with an average thickness between 1 and 3 layers (estimated from XPS characterization across a large area (5mm2 sample). The graphene layer thickness is obtained from monitoring changes in intensity of the Si2p SiC substrate peak and also the SiC bulk and graphene C1s peaks during the graphene growth process.

Assuming the graphene growth follows a Franck van der Merwe growth or layer-by-layer mode [38], the intensity of the Si2p and SiC bulk C1s peaks decay exponentially as a function of the mean free path and over layer (graphene layer) thickness. Thus a study of these XPS peaks can be used to extract the average graphene layer thickness over the scanned sample area, using the method detailed by Fadley *et al.,* [39], which according to Biedermann *et al.,* [40], can be used to calculate the thickness of a graphene over layer from the ratio of the intensity of the graphitic component from the graphene over layer, and the intensity of the bulk SiC component.

Figure 2 shows two XPS spectra from the same sample. The first spectrum Figure 2(a) was recorded with the sample normal to the electron analyser. The sample was subsequently tilted to 60° from the normal orientation, halving the mean free path (MFP), and allowing determination of the MFP value. By curve fitting to these C1s spectra, the contribution of the C1s peak from the SiC bulk component and surface graphene component was inferred.

From this data, along with the Si2p spectra, an average graphene layer thickness of more than 1 graphene layer was found to be present on the SiC surface. The graphene layer thickness is inhomogeneous across the sample, with some regions of the SiC substrate covered with 1 graphene layer whilst others are covered by up to 3 layers. However, repeatable growth of uniform 1-3 layer graphene (few layer graphene, FLG) on C-face SiC is difficult to achieve. Uniform multi-layer graphene growth, with an average of around 6 layers in thickness (multi-layer epitaxial graphene, MLEG), is more repeatable and has more consistent electronic properties than 1-3 layer graphene. For this reason, MLEG has been used in the functionalisation of graphene sensor devices. In MLEG, the C1s peak in the XPS spectrum consists predominantly of the graphene component, as the C1s peak of the bulk SiC substrate is buried beneath the graphene peak.

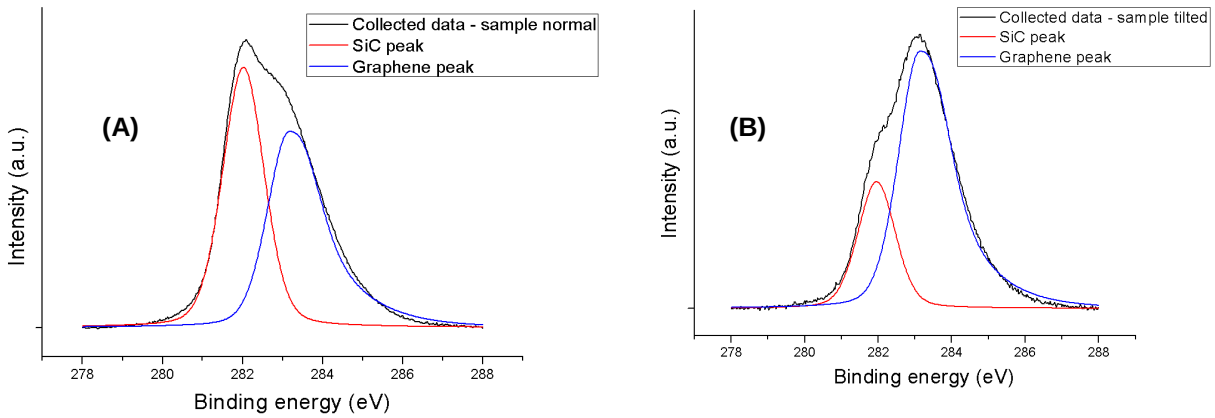

Figure 2: XPS spectra of the C1S peak of a 1-3 layer graphene (averaged over the sample) / 4H-SiC sample, obtained with the electron analyser positioned perpendicular to the sample (2.A), and tilted 60° from the normal orientation (2.B), respectively. The measured data (black curves) are curve fitted to show the SiC bulk (red curves) and graphene (blue curves) component of the peaks. The larger graphene peak in the tilted configuration illustrates the increase in surface sensitivity of the 60° scan.

Raman spectroscopy can be used to characterize the thickness and quality of the epitaxial graphene grown on 4H-SiC (Figure 3). In general, the number of graphene layers can be inferred from the shape of the graphene 2D band. However, in the case of graphene grown on the C face of 4H-SiC, this is a poor indicator of the number of graphene layers, as turbostratic growth of graphene layers on the C face causes electronically decoupled layers [41]. This can cause multilayer C-face graphene to have a 2D band similar to the case of a single graphene monolayer[42].

The MLEG sample features a large D band which is due to the presence of sp^3 bonds that originate from lattice defects in the layers. To minimize any contribution from the channel edges, the Raman spectra were acquired from a laser spot positioned well within the micro-channel (away from the edges).

The D-band has lower intensity in the 1-3 layer graphene, suggesting a slightly lower defect concentration. In both samples, the majority of the graphene lattice consists of sp^2 bonded carbon atoms.

The presence of the SiC substrate has a significant effect on the peak positions and shapes in the Raman spectra of epitaxial graphene, in comparison to exfoliated graphene (free-standing or on SiO2). This effect can be related to the charge doping and strain effects from the SiC substrate [43]. The SiC substrate contributes a large background signal to the Raman spectrum. For clarity, the SiC Raman background has been removed from the presented Raman data, thus highlighting the Raman contributions from the top most graphene layers. The attenuation of the SiC background in the Raman spectra can be used as an approximate indicator of the number of graphene layers [44] Raman spectra were measured under ambient conditions with a 50X objective focused in the middle of the graphene channels, such that the focus was entirely within the graphene channel. The incident laser power was ~11 mW and the wavelength was 532 nm for Figures (3, 7) and 785 nm for Figure 6. Care

was taken to obtain spectra from repeatable points to ensure that differences in the D-band intensity were attributed to differences in the sample area scanned.

It has been reported that the quality of the graphene and information relating to its doping may also be inferred from Raman shifts of the G and 2D band. However, substrate effects also have an impact on the Raman shifts in epitaxial graphene and add increased complexity to any analysis of doping effects.

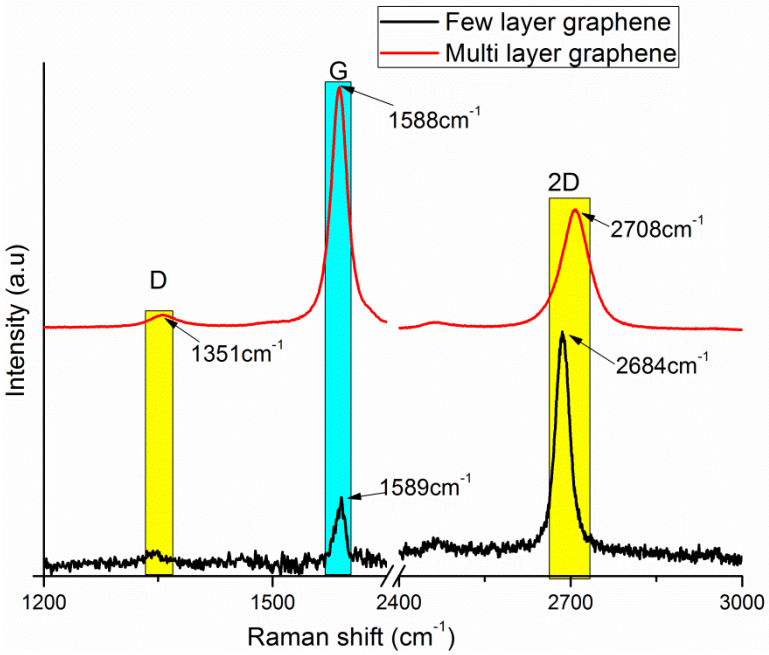

Figure 3: Raman spectra of few layer (1-3 Layers on average) and multi-layer (6-10 Layers on average) epitaxial graphene with the D, G, and 2D peaks highlighted (individual spectra have been offset vertically for clarity).

3.2. Characterization of surface functionalisation by electrochemistry

Cyclic voltammetry has been performed on graphene channel before expouse to a diazonium salt solution (Figure 4, curve A). This curve indicates no redox reaction taken place. The early stages of the reaction after the application of diazonium salt (Figure 4, curve B) shows a large reduction peak, related to the irreversible attachment of the nitro-phenyl radical to the graphene electrode surface. The latter stages of this reduction reaction (Figure 4, curve C) show the attachment reaction is virtually complete, and the surface is saturated with nitro-phenyl groups. The attachment of the nitro-phenyl group was performed using CV, which was also used to monitor the progress of the attachment reaction. Nitro-phenyl attachment

was followed by subsequent reduction of the nitro (NO_2) group to an amine (NH_2). The reduction step is performed in 0.1M KCl / Ethanol (9:1) solution using chronoamperometry. From CV measurements the optimum voltage for reduction of the nitro- phenyl group to phenyl amine was determined as -0.9V. Therefore, a constant voltage of -0.9V was applied between the Ag/ AgCl and the graphene working electrode for 500 seconds until a stable current was achieved (Figure 4, inset bottom right). This indicates that the reduction reaction is near completion.

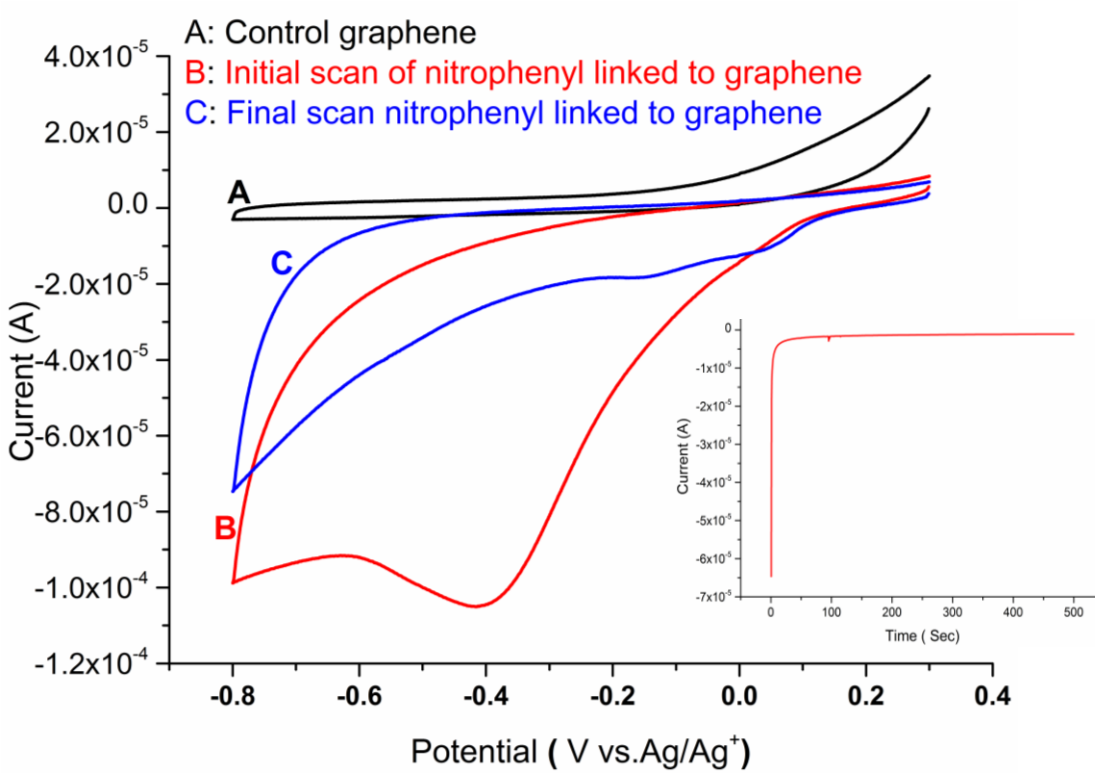

Figure 4: Cyclic voltammograms (A) control sample (non-functionalised graphene) in non-aqueous electrolyte (Bu_4NBF_4 in acetonitrile) with no diazonium reagent present (black curve); (B) functionalisation of the graphene surface with the nitro-aryl diazonium salt (red curve); (C) after repeated voltammetry cycles (5 cycles) the functionalisation process is near completion and the graphene surface is saturated with the surface-attached nitro-phenyl (blue curve). Reduction step is performed in 0.1M KCl / Ethanol (9:1) solution using chronoamperometry, a constant voltage was applied between the Ag/ AgCl and the graphene working electrode (inset, bottom right).

3.3. Characterization of graphene functionalisation by X-ray photoelectron spectroscopy and Raman

Nitro -phenyl functionalisation and subsequent reduction to phenyl amine has been confirmed using XPS. No N1S peak was present before functionalisation. After nitro-phenyl attachment, monitoring of the N 1s peak shows the graphene-attached nitro and amine groups at different binding energies. After nitro-phenyl functionalisation, a single N1s peak at 404.6 eV, with a shoulder at lower binding energy, was present in the XPS spectrum. The shoulder peak is thought to be comprised of NHOH and NH_2 groups. Following electrochemical reduction of the nitro-phenyl group, a clear peak at 398.7 eV, attributed to phenyl amine, is seen – in addition to the nitro-phenyl peak at 404.6eV, as shown in Figure 5.

The consequence of the electrochemical reduction of the nitro group is that the relative surface coverage of phenyl amine groups increases from less than 20% to over 40%. Incomplete reduction of nitro-phenyl to yield phenyl amine-functionalised surfaces has also been reported for reduction of nitro-phenyl groups on glassy carbon electrodes [45]. Optimisation of the electrolyte and use of a catalyst can be used to improve the conversion of NO_2 to NH_2 groups [46]. In this work 40% NH_2 coverage was sufficient for successful bio-attachment of the 8-OHdG antibody.

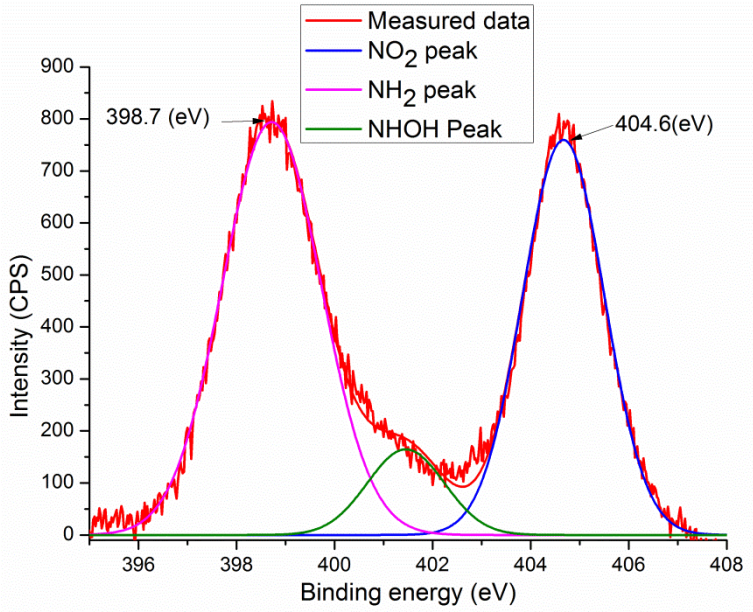

Figure 5: X-ray photoelectron spectroscopy (XPS) spectrum of the functionalised graphene channel after partial reduction of the $PhNO_2$ to $PhNH_2$. Clear N1s peaks, attributed to NO_2 (404.6 eV) and NH_2 (398.7 eV), respectively indicate partial reduction of the attached nitro-phenyl group.

The raman spectra in Figure 6 illustrate the changes to a MLEG sample as a result of the functionalisation with phenyl amine ($PhNO_2$/$PhNH_2$). An enhanced D band peak at around 1360cm^{-1} is observed upon functionalisation. The enhanced D-peak is related to an increase in the conversion of sp^2 hybridized carbons to a sp^3 carbon atoms [47]. The D-band is due to the A1g breathing mode vibrations of six-membered sp^2 carbon rings, and becomes Raman active after neighbouring sp^2 carbons are converted to sp^3 hybridization in graphitic materials. This peak appears to substantiate the XPS data and indicates covalent attachment of aniline groups has occurred. It has been demonstrated in the literature that non-covalent adsorption of nitro- phenyl molecules does not result in the formation of a D band but results in a doping effect on the graphene[48].

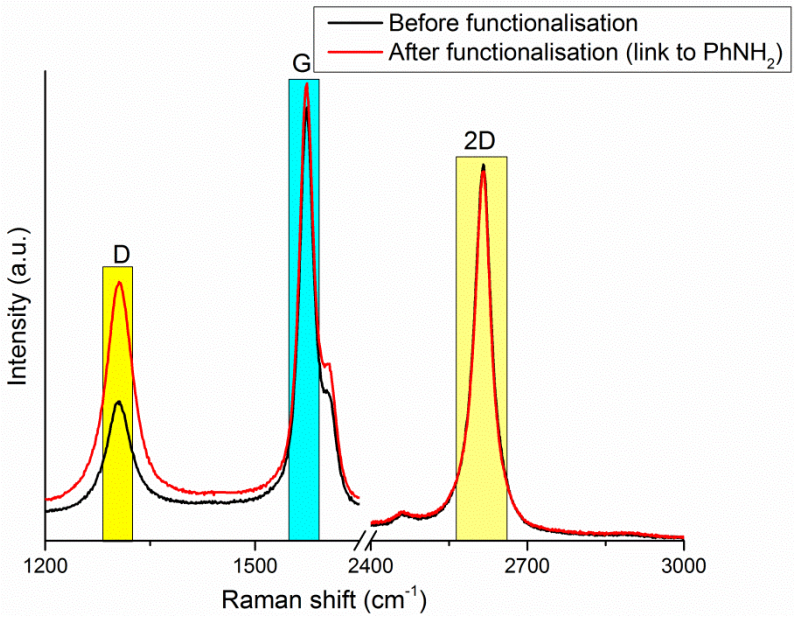

Figure 6: Spectra demonstrating overall effect, including increased D band intensities, of functionalisation on multi-layer epitaxial graphene.

Further Raman studies were conducted to specifically consider the effect of the reduction process and this can be seen in Figure 7 which compares the $PhNO_2$ attachment with the $PhNH_2$. In addition to the graphene D band at 1360 to 1375 cm^{-1} functionalised surface. The NO_2 stretch is also found at around 1360cm^{-1}. Moreover a band from the C–N vibration of 4-phenyl amine is found at 1372 cm^{-1}. It is possible that all these Raman signals may contribute to the observed the peak in the spectrum from 1360 to 1372 cm^{-1}leading to a change in peak shape and position. However the peak in this region of the spectrum is dominated by the

underlying graphene D peack. The higher wave number region has been magnified to show the effects on the D+D* peak, this peak is also attributed to defects in graphene [48].

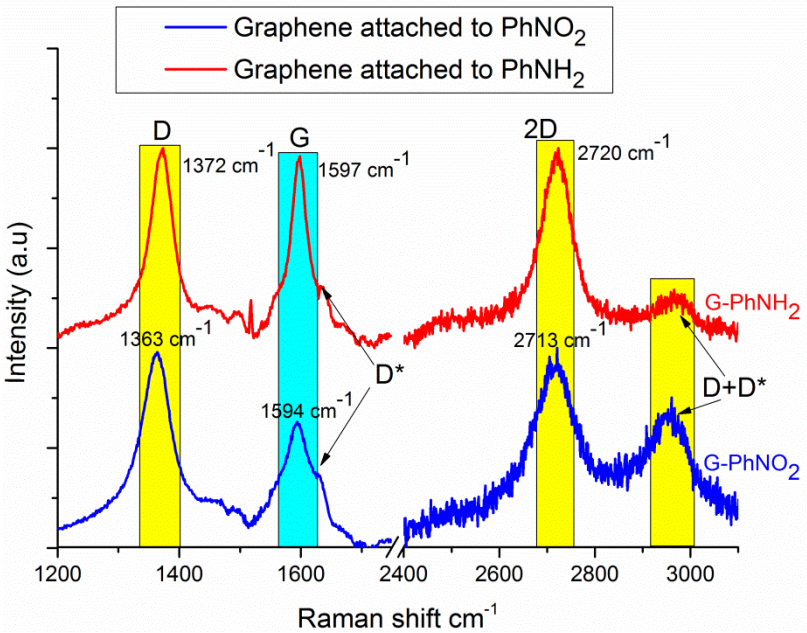

Figure 7: Comparison of Raman bands for nitro-phenyl functionalised epitaxial graphene and phenyl amine functionalised epitaxial graphene. The intensity has been separately scaled for clarity.

The G band peak at 1590-1600 cm $^{-1}$ is attributed to C–C vibrations and may contain components from the benzene ring of the nitro-phenyl group, but again will be dominated by Raman signals from the sp^2 C-C bonds in the graphene layer.

Comparison of the D, G and 2D bands in phenyl amine functionalised graphene with the bands in nitro-phenyl functionalised graphene, reveals that all the phenyl amine bands are slightly blue-shifted relative to nitro-phenyl functionalised graphene. The spectra reveals a D* band at ~1630 cm^{-1} and a D + D* band at ~2965cm^{-1} which are both attributable to defects in the underlying graphene and occur in both the nitro-phenyl and phenyl amine functionalised graphene. Features in the Raman spectra of functionalised graphene are dependent on the quality and thickness of the starting graphene, but observable differences in the spectra shown in Figure 7 reflect changes seen on the same graphene channel and indicate a response in the graphene signature spectra to the conversion of the nitro-phenyl group to phenyl amine.

3.4. Fluorescence verification of binding of second antibody labelled Q-Dot on the Epitaxial Graphene

The amino groups of the surface-bound phenyl amine can subsequently be used to attach "bioreceptor" antibodies to the graphene channel. This binding may be covalent, using an interaction of the NH_2 group with the COOH group of the biomolecules - resulting in a covalent amide bond. Alternatively, the binding may be electrostatic. Attachment of a primary antibody, targeted against 8-OHdG, to the graphene surface has been verified by binding a fluorescently labeled secondary antibody to the primary antibody (see detail in methods section).

Fluorescence from the attached labeled secondary antibody was detected using confocal fluorescence microscopy. Graphene devices with micron- sized channels were fabricated and functionalised as described above. Fluorescence from the labelled secondary antibodies was detected only from the region of the graphene channel as shown in Figure 8, which indicates that the primary antibody is bound to the graphene channel and not the silicon carbide substrate. Inspection of the antibody-functionalised graphene surface, after (i) primary antibody attachment and blocking with BSA, washing (ii) subsequent Qdot-labelled secondary antibody attachment to the primary antibody functionalised surface and washing, the final functionalised surface exhibited strong fluorescence. This indicates that both the primary and secondary antibodies are still present and indeed strongly bound to the functionalized graphene surface.

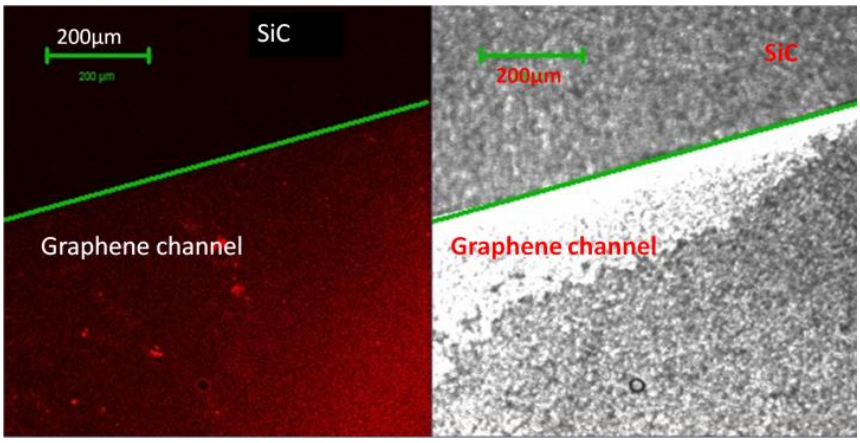

Figure 8: Confocal fluorescence (left) and optical (right) microscopy images of aniline-modified graphene channels after exposure to Q-Dot labelled antibodies. Areas where the labeled antibodies are bound to the surface appear red. Areas where the antibodies are not bound appear dark.

3.5. AFM surface analysis

The effect of surface functionalisation of graphene with amine linking group has been monitored using AFM. The surface roughness of graphene substrates before functionalisation (Figure 9) shows the change in surface topography related to the attachment of $PhNH_2$ compounds to the graphene surface. The AFM images show clear differences between clean and modified surface in terms of surface topography. The graphene surface is observed to be atomically flat and uniform with typical RMS (Root Mean Square) roughness measurements of 0.22 nm before functionalisation (Figure 9A). Attachment of $PhNH_2$ compounds to the graphene resulted in a marked change in the surface topography; modified surfaces had an RMS roughness of 0.44 nm (Figure 9B). The surface RMS roughness is increased to 0.96 nm following surface-attachment of the antibody, as shown in Figure 9C.

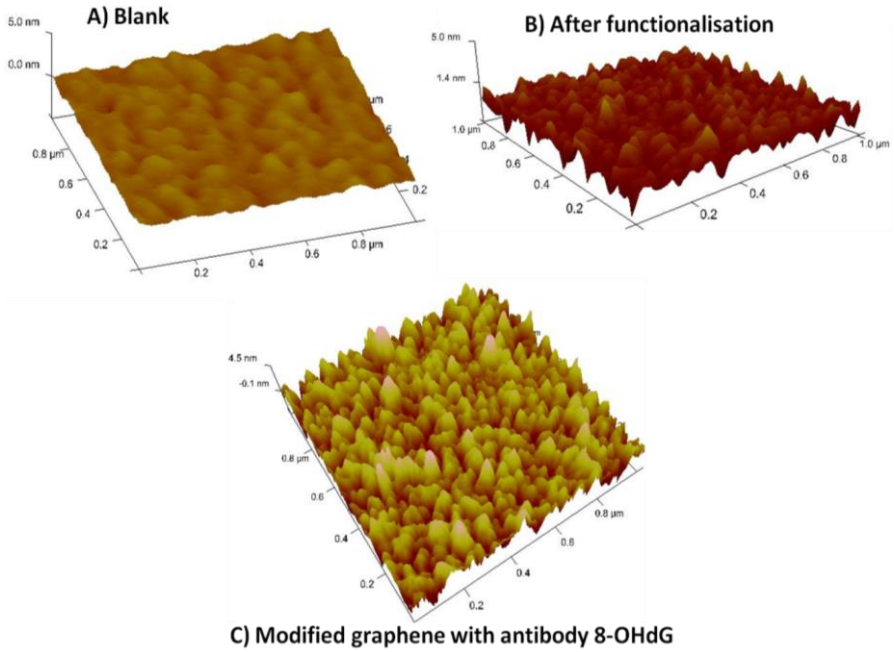

Figure 9: AFM topography images of graphene surfaces. Topography images acquired (A) prior to functionalisation, (B) after surface functionalisation with $PhNO_2$/$PhNH_2$ and (C) after attachment with targeted biomarker, anti (8-OHdG). AFM acquisitions demonstrate clear differences in surface roughness following functionalisation of the graphene surface.

3.6. Electrical characterisation and detection of biomolecule

The electrical behavior of graphene channel devices has been monitored at each stage of the functionalisation process; measured as a current-voltage signal as shown in Figure 10. The initial nitro-phenyl attachment results in reduced current transport (at 1V, the current is reduced from 119 mA to 42 mA) through the graphene channel, consistent with conversion of sp^2 to sp^3 hybridized bonds and reduced mobility through decreased sp^2 delocalisation and increased scattering sites [49].

A decrease in graphene conductivity was also observed by Bekyarova *et al.,* [15], who observed a doubling of the graphene resistance upon grafting of nitro-phenyl groups on to epitaxial graphene. A similar effect was reported for the covalent attachment of 4-nitro-phenyl groups to graphene nano ribbons [49].

Work on graphene nanoribbons has shown that the edge of the nanoribbons is at least twice as reactive as the bulk graphene plane [50]. This suggests that there may be increased functionalisation at the edges of the graphene channel in our device.

Graphene and CNT functionalisation has been reported to reduce conductivities. For example, nitro- phenyl functionalisation chemistry has previously been used to modify the electronic properties of single-walled carbon nanotubes (SWNT) from metallic to semiconducting [51]. Whilst functionalisation of graphene, creating defective insulating or semiconducting regions on graphene, has been be used to pattern graphene transistor devices [52].

Reduction of the nitro- phenyl group to phenyl amine results in a further decrease in channel conductivity (Figure 10A). This may be explained by the increased electron donation from the phenyl amine group, compared to the nitro-phenyl group. In p-type graphene this electron donation could effectively reduce the density of p-type carriers. Epitaxial graphene, grown on the C-face of 4H-SiC, has been reported to be p-type doped, so reduced conductivity of graphene related to increased electron donation is consistent with the observed I-V characteristics. Attachment of the antibody yields an increase in channel conductivity relative to the $PhNH_2$ surface.

The effect of electron withdrawing and electron donating moieties on graphene has previously been discussed by Huang *et a*l. [35]. They claimed that the method of covalently attaching aryl groups to a graphene basal plane can tune the conductivity of graphene either to a higher or lower level depending on the quantity of aryl groups bonding to graphene.

Antibody attachment to the phenyl amine functionalised graphene channel results in an increase in the channel conductivity, relative to the conductivity of the phenyl amine functionalised channel (Figure 10B) [53]. The negatively charged antibody would be expected to enhance the conductivity in a p-type graphene channel. The attachment of the negatively charged antibody is equivalent to a negative potential gating of the graphene channel, which if the graphene were p-type, would increase the carrier density and thus the conductivity in the device. Analogous sensing mechanisms have been outlined in [54] for the detection of negatively charged bacterium to a p-type graphene amine surface, whereby the hole current was increased by the negative gating potential. The final detection step, is an electrical response to binding of the target 8-OHdG biomarker to the "bioreceptor" antibody, (Figure 10B), yielding an increase in the current though the sensor channel (Figure 10C).

This current modulation could be related to further changes in charge density in the vicinity of the graphene channel, due to binding of the target biomarker with the antibody.

Crucially, non-modified graphene control samples showed no change when exposed to the target biomarker and thus only the antibody functionalised sensor-produces a current response on expose to the target biomolecule. Five comparable devices were fabricated and functionalised, as outlined in Experimental section. The electrical behavior was consistent and repeatable for each characterized device, indicating that 8-OHdG can be repeatedly and reliably detected in PBS solutions at a concentration of 20 nM. This concentration range clinically relevant to detection of 8-OHdG in urine, and its reported relation to prostate cancer risk [33].

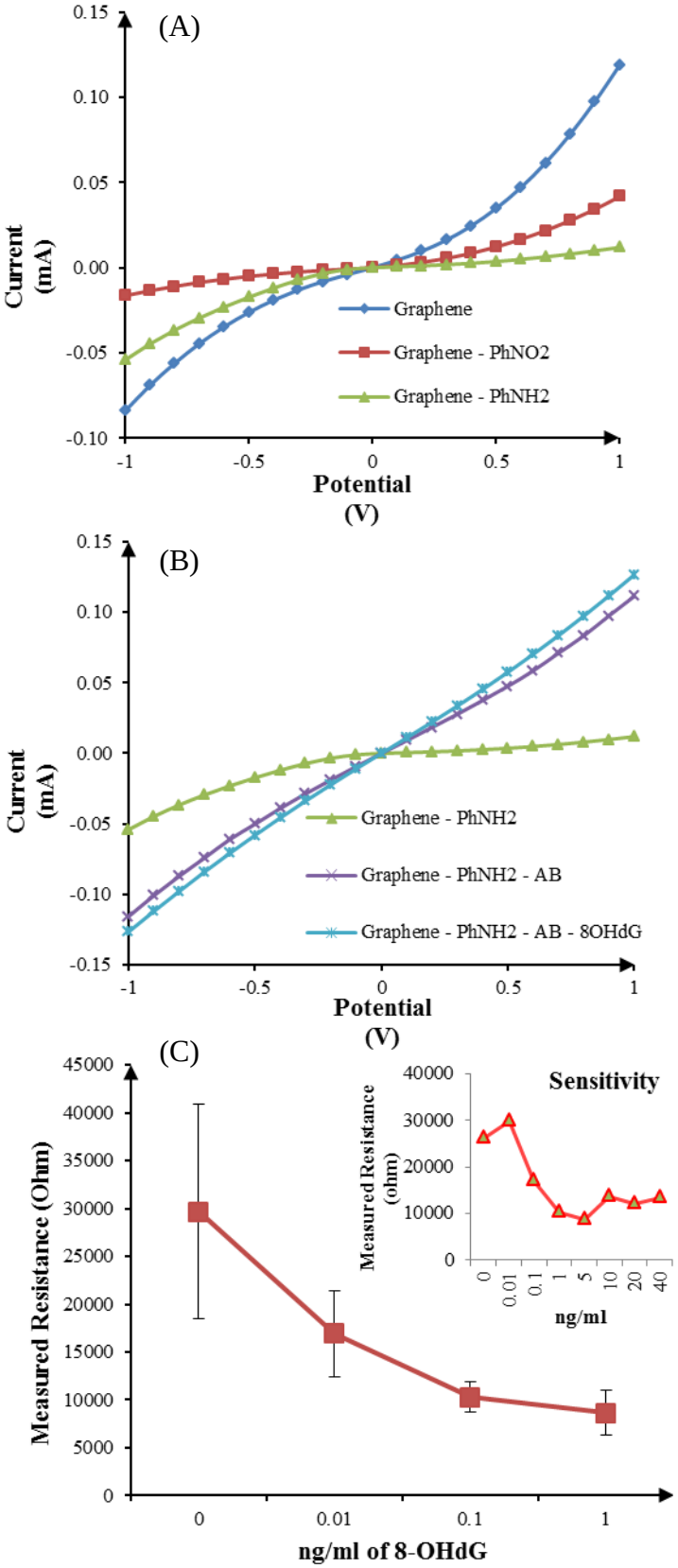

Figure 10: A) I-V characteristics of the graphene channel, blue: before functionalisation red: after electrochemical attachment of nitro-phenyl green: after reduction to phenyl amine B) I-V characteristics of the amine functionalised graphene channel purple: after attachment to the antibody 8-OHdG: after attachment to the target biomarker (light blue). C) I–V curves for MLEG, response of an antibody MLEG biosensor device to increasing concentrations of 8-OHdG antigen (0.1ng / ml to 20 ng /ml).

The detection mechanism is observed appears similar to that of graphene chem-FETs. Defective graphene, and graphene influenced by extrinsic defects from the substrate is reported to be particularly sensitive to potential gating effects [55], whereas pristine (defect-free) graphene is not strongly sensitive. The presence of defects in graphene causes the current modulation from chemical gating to be enhanced, translating into superior sensitivity in chem-FETs. Graphene grown on the C face of SiC is not a flat, uniform layer, but instead commonly grows into step-bunched terraces[55]. It is likely that structural defects from the epitaxial graphene growth, and chemical defects from the diazotization step, both contribute to the sensitivity of the current modulation in response to binding of the antibody.

Exposure of the antibody functionalised graphene sensor to the 8-OHdg antigen acts to decrease the resistance across the channel. Indeed, increasing the concentration of 8-OHdG results in further decreases in the graphene channel resistance, indicating that 8-OHdG was bound to the sensor. After exposure to concentrations above 5ng/mL, the sensor response saturated, indicating that the active receptor sites had been occupied by the bound antigens. The limit of detection was determined as 0.1ng/ml.

4. Conclusion

A key part of any biosensor technology is surface functionalisation. Functionalisation of graphene channels was achieved in a matter of minutes, using an electrochemical diazotization method for nitro phenyl attachment to graphene channel and a subsequent reduction process, converting the nitro group to an amine, under mild conditions. This represents a far more effective and production friendly process than any other reported diazotization. The advantage of this functionalisation method over previously reported techniques [15, 34, 35], lies in its simplicity, avoidance of harsh oxidation chemistry and speed of reaction.

Characterisation of functionalised surfaces using XPS, Raman measurements and AFM have been used to confirm attachment of nitro- phenyl and amino phenyl groups to the graphene channel. AFM showed that surface roughness of graphene increased after surface modification with nitro- phenyl or amino phenyl groups. Laser Scanning Confocal Microscopy (LSCM) has been used to verify subsequent biofunctionalisation of the graphene channel, using fluorescently labelled antibodies. Antibody attachment occurs only at the graphene channels and not on the SiC substrate.

Changes in conductivity of the channel devices were observed at each stage of the functionalisation process. The critical detection step; binding of the target 8-OHdG biomarker, (which has been related to prostate cancer risk), to the epitaxial graphene-bound "bioreceptor" antibody, yielded a detectable decrease in the graphene channel resistance.

Diazotization of epitaxial graphene in order to attach antibody bioreceptors has been used in this work, and it is capable of selectively detecting of the oxidative stress biomarker 8-OHdG. This epitaxial graphene biosensor device has been demonstrated to be capable of detecting 8-OHdG concentrations as low as 0.1 ng/mL in a faster and more sensitive method (5 times lower LOD), compared with ELISA tests [33]. Since the attachment mechanism uses non-specific sites of the antibody (i.e. carboxylic groups) to bond to the NH_2 terminated surface, this method could potentially be adapted to attach other antibodies for the detection of other biomarkers. Thus, epitaxial graphene channel devices offer an easily adaptable, generic sensing platform for detection of a range of target biomarkers and thus be used in sensors for early diagnosis and monitoring for a variety of diseases.

In summary, an electrochemical functionalisation method for epitaxial graphene channel devices has been demonstrated. Phenyl amine functionalised epitaxial graphene has been used to attach antibody bioreceptors to graphene channels.
The antibody based sensors have been used to detect nM concentrations of the oxidative stress biomarker, 8-OHdG. The sensor displayed a specific and selective response to the 8-OHdG target biomarker.
No electrical response was detected on exposure to control solutions, not containing 8-OHdG.
The electrical response of the functionalised channels to the 8-OHdG analyte in test PBS solutions is complete in a matter of minutes, allowing rapid qualitative detection of the disease biomarker analyte.

5. Acknowledgements

This work was supported by the Engineering and Physical Science Research Council [grant number EP/I00193X/1].

6. Abbreviations

Enzyme-Linked Immunobsorbant Assays, (ELISAs); Silicon Carbide (SiC); (Few Layer Graphene (FLG); X-ray photoelectron spectroscopy (XPS); Cyclic Voltammetry (CV); Carbon Nanotubes (CNT); Single-Walled Carbon Nanotubes (SWNT); Electron-Beam Lithography (EBL); Acetonitrile (ACN); Highly Ordered Pyrolytic Graphite (HOPG); Mean Free Path (MFP); nitro-phenyl group (Ph-NO_2); 8-hydroxydeoxyguanosine (8-OHdG); Laser Scanning Confocal Microscopy (LSCM).

7. References

1. Gomez De Arco, L., Zhang, Yi., Schlenker, C. W., Ryu, K., Thompson, M.E. Zhou, C.,, *Continuous, highly flexible, and transparent graphene films by chemical vapor deposition for organic photovoltaics.* Acs Nano, 2010. **4**(5): p. 2865-73.
2. Kim, K.S., Zhao, Y., Jang, H., Lee, S. Y., Kim, J. M., Ahn, J. H., Kim, P., Choi, J. Y., Hong, B. H., *Large-scale pattern growth of graphene films for stretchable transparent electrodes.* Nature, 2009. **457**(7230): p. 706-710.
3. Wang, Y., Shao, Y., Matson, D. W., Li, J., & Lin, Y. , *Nitrogen-doped graphene and its application in electrochemical biosensing.* ACS nano, 2010. **4**: p. 1790–1798.
4. Schedin, F., Geim, A. K., Morozov, S. V., Hill, E. W., Blake, P., Katsnelson, M. I., & Novoselov, K. S., *Detection of individual gas molecules adsorbed on graphene.* Nature Materials, 2007. **6**(9): p. 652-655.
5. Wu, Y.Q., Lin, Y. M., Bol, A. A., Jenkins, K. A., Xia, F. N., Farmer, D. B., Zhu, Y., Avouris, P., *High-frequency, scaled graphene transistors on diamond-like carbon.* Nature, 2011. **472**(7341): p. 74-78.
6. Yang, H., Heo, J., Park, S., Seo, D. H., Byun, K. E., Kim, P., Yoo, I., Chung, H. J., Kim, K., *Graphene Barristor, a Triode Device with a Gate-Controlled Schottky Barrier.* Science, 2012. **336**(6085): p. 1140-1143.
7. Liao, L., Lin, Y. C., Bao, M. Q., Cheng, R., Bai, J. W., Liu, Y. A., Qu, Y. Q., Wang, K. L., Huang, Y., Duan, X. F., *High-speed graphene transistors with a self-aligned nanowire gate.* Nature, 2010. **467**(7313): p. 305-308.
8. Lin, Y.M., Dimitrakopoulos, C., Jenkins, K. A., Farmer, D. B., Chiu, H. Y., Grill, A., Avouris, P., *100-GHz Transistors from Wafer-Scale Epitaxial Graphene.* Science, 2010. **327**(5966): p. 662-662.
9. Castaing, A., O.J. Guy, M. Lodzinski, S.P. Wilks,, *Investigation of Graphene Growth on 4H-SiC.* Mater. Sci, 2009. **615-617**: p. 223-226.
10. Yang, W.R., Ratinac, K. R., Ringer, S. P., Thordarson, P., Gooding, J. J., Braet, F., *Carbon Nanomaterials in Biosensors: Should You Use Nanotubes or Graphene?* Angewandte Chemie-International Edition, 2010. **49**(12): p. 2114-2138.
11. Loh, K.P., Bao, Q. L., Ang, P. K., Yang, J. X., *The chemistry of graphene.* Journal of Materials Chemistry, 2010. **20**(12): p. 2277-2289.
12. Bahr, J.L., Yang, J. P., Kosynkin, D. V., Bronikowski, M. J., Smalley, R. E., Tour, J. M., *Functionalization of carbon nanotubes by electrochemical reduction of aryl diazonium salts: A bucky paper electrode.* Journal of the American Chemical Society, 2001. **123**(27): p. 6536-6542.
13. Englert, J.M., Dotzer, C., Yang, G. A., Schmid, M., Papp, C., Gottfried, J. M., Steinruck, H. P., Spiecker, E., Hauke, F., & Hirsch, A., *Covalent bulk functionalization of graphene.* Nature Chemistry, 2011. **3**(4): p. 279-286.
14. Shih, C.J., Wang, Q. H., Jin, Z., Paulus, G. L. C., Blankschtein, D., Pablo,J.-H., Strano, M. S.,, *Disorder imposed limits of mono- and bilayer graphene electronic modification using covalent chemistry.* Nano letters, 2013. **13**(2): p. 809-17.
15. Bekyarova, E., Itkis, M. E., Ramesh, P., Berger, C., Sprinkle, M., de Heer, W. A., Haddon, R. C., *Chemical Modification of Epitaxial Graphene: Spontaneous Grafting of Aryl Groups.* Journal of the American Chemical Society, 2009. **131**(4): p. 1336-+.
16. Yan, L., Zheng, Y. B., Zhao, F., Li, S., Gao, X., Xu, B., Weiss, P. S., & Zhao, Y., *Chemistry and physics of a single atomic layer: strategies and challenges for functionalization of graphene and graphene-based materials.* Chem. Soc. Rev, 2011. **41**: p. 97–114.
17. Lomeda, J.R., Doyle, C. D., Kosynkin, D. V., Hwang, W. F., Tour, J. M., *Diazonium Functionalization of Surfactant-Wrapped Chemically Converted Graphene Sheets.* Journal of the American Chemical Society, 2008. **130**(48): p. 16201-16206.
18. Lim, H., Lee, J. S., Shin, H. J., Shin, H. S., Choi, H. C., *Spatially Resolved Spontaneous Reactivity of Diazonium Salt on Edge and Basal Plane of Graphene without Surfactant and Its Doping Effect.* Langmuir, 2010. **26**(14): p. 12278-12284.
19. Balog, R., Jorgensen, B., Nilsson, L., Andersen, M., Rienks, E., Bianchi, M., Fanetti, M., Laegsgaard, E., Baraldi, A., Lizzit, S., Sljivancanin, Z., Besenbacher, F., Hammer, B., Pedersen, T. G., Hofmann, P., Hornekaer, L., *Bandgap opening in graphene induced by patterned hydrogen adsorption.* Nature Materials, 2010. **9**(4): p. 315-319.
20. Boukhvalov, D.W., and M I Katsnelson, *Chemical functionalization of graphene.* J. Phys.: Condens. Matter 2009. **21**: p. 344205.
21. Elias, D.C., R.R. Nair, T.M.G. Mohiuddin, S.V. Morozov, P. Blake, M.P. Halsall, A.C. Ferrari, D.W. Boukhvalov, M.I. Katsnelson, A.K. Geim, & K.S. Novoselov, *Control of Graphene's Properties by Reversible Hydrogenation: Evidence for Graphene.* SCIENCE, 2009. **323**.
22. Roman, T., Dino, W. A., Nakanishi, H., Kasai, H., Sugimoto, T., & Tange, K. , *Hydrogen pairing on graphene.* Carbon 2007. **45**: p. 203–228.
23. Ruoff, R., *Graphene: Calling all chemists.* Nature nanotechnology, (2008. **3**: p. 10–11.
24. Wei, Z., Wang, D., Kim, S., Kim, S. Y., Hu, Y., Yakes, M. K., Laracuente, A. R., Dai, Z., Marder, S. R., Berger, C. , *Nanoscale tunable reduction of graphene oxide for graphene electronics.* Science, 2010. **328**: p. 1373–1376.
25. Pumera, M., Ambrosi A., , *Graphene for electrochemical sensing and biosensing. TrAC Trends in Analytical Chemistry* **2010**. **29**(9).
26. Adenier, A., M.-C. Bernard, M. M. Chehimi, E. Cabet-Deliry, B. Desbat, O. Fagebaume, J. Pinson and F. Podvorica, *Covalent modification of iron surfaces by electrochemical reduction of aryldiazonium salts.* Journal of the American Chemical Society, 2001. **123**(19).
27. Delamar, M., Hitmi, R., Pinson, J., & Saveant, J. M. , *Covalent modification of carbon surfaces by grafting of functionalized aryl radicals produced from electrochemical reduction of diazonium salts.* Journal of the American Chemical Society 1992. **114**: p. 5883–5884.
28. Erhola, M., Toyokuni, S., Okada, K., Tanaka, T., Hiai, H., Ochi, H., Uchida, K., Osawa, T., Nieminen, M. M., Alho, H., KellokumpuLehtinen, P., *Biomarker evidence of DNA oxidation in lung cancer patients: Association of urinary 8-hydroxy-2'deoxyguanosine excretion with radiotherapy, chemotherapy, and response to treatment.* Febs Letters, 1997. **409**(2): p. 287-291.
29. Valavanidis, A., Vlachogianni, T., & Fiotakis, C., *8-hydroxy-2' -deoxyguanosine (8-OHdG): A Critical Biomarker of Oxidative Stress and Carcinogenesis.* Journal of Environmental Science and Health Part C-Environmental Carcinogenesis & Ecotoxicology Reviews, 2009. **27**(2): p. 120-139.
30. Wu LL, C.C., Chang PY, Wu JT, *Urinary 8-OHdG: a marker of oxidative stress to DNA and a risk factor for cancer, atherosclerosis and diabetes.* Clin Chim Acta, 2004. **339**: p. 1-9.
31. Makarov, D., V., Stacy Loeb, Robert H. Getzenberg, & Alan W. Partin, *Biomarkers for Prostate Cancer.* The Annual Review of Medicine, 2009. **60**: p. 139-51.
32. Stangelberger, A., Margreiter, M., Seitz, C., & Djavan, B., *Prostate cancer screening markers.* The journal of men's health & gender, 2007. **4**: p. 233–244.
33. Chiou, C.C., Chang, P. Y., Chan, E. C., Wu, T. L., Tsao, K. C., Wu, J. T., *Urinary 8-hydroxydeoxyguano sine and its analogs as DNA marker of oxidative stress: development of an ELISA and measurement in both bladder and prostate cancers.* Clinica chimica acta, 2003. **334**(1-2): p. 87-94.

34. Pinson, J., & F. Podvoricab *Attachment of organic layers to conductive or semiconductive surfaces by reduction of diazonium salts.* Chem. Soc. Rev, 2005. **34**.
35. Huang, P., Zhu, H. R., Jing, L., Zhao, Y. L., Gao, X. Y., *Graphene Covalently Binding Aryl Groups: Conductivity Increases Rather than Decreases.* Acs Nano, 2011. **5**(10): p. 7945-7949.
36. Koehler, F.M., Stark, W. J., *Organic Synthesis on Graphene.* Accounts of Chemical Research, 2013. **46**(10): p. 2297-2306.
37. Ko, G., Kim, H.-Y., Ahn, J., Park, Y.-M., Lee, K.-Y., & Kim, J. , *Graphene-based nitrogen dioxide gas sensors.* Current Applied Physics, 2010. **10**: p. 1002–1004.
38. Bauer, E., *Phänomenologische Theorie der Kristallabscheidung an Oberflächen. II* Zeitschrift für Kristallographie, 1958. **110**: p. 395-43.
39. Kono, S., Fadley, C.S., Hall, N.F.T., Hussain, Z., *Azimuthal anisotropy in core-level X-ray photoemission from c (2 × 2) oxygen on Cu (0 0 1): experiment and single-scattering theory.* Physical Review Letters 1978. **41**(2): p. 117.
40. Biedermann, L.B.B., M. L. Capano, M. A. Zemlyanov, D. Reifenberger, R. G., *Insights into few-layer epitaxial graphene growth on 4H-SiC(000(1)over-bar substrates from STM studies.* Physical Review B, 2009. **79**(12).
41. Hass, J.V., F. Millan-Otoya, J. E. Sprinkle, M. Sharma, N. De Heer, W. A. Berger, C. First, P. N. Magaud, L. Conrad, E. H., *Why multilayer graphene on 4H-SiC(000(1)over-bar) behaves like a single sheet of graphene.* Physical Review Letters, 2008. **100**(12).
42. Faugeras, C.N., A. Potemski, M. Mahmood, A. Dujardin, E. Berger, C. de Heer, W. A., *Few-layer graphene on SiC, pyrolitic graphite, and graphene: A Raman scattering study.* Applied Physics Letters, 2008. **92**(1).
43. Lee, D.S., Riedl, C., Krauss, B., Von Klitzing, K., Starke, U., & Smet, J. H. , *Raman spectra of epitaxial graphene on SiC and of epitaxial graphene transferred to SiO2.* Nano letters, 2008. **8**: p. 4320–4325.
44. Shivaraman, S., Chandrashekhar, M., Boeckl,J. J. and Spencer, M. G. , *Thickness estimation of epitaxial graphene on sic using attenuation of substrate raman intensity.* Journal of electronic materials, 2009. **38**(6): p. 725-730.
45. Nazemi, Z., Shams, E., & Amini, M. K., *Covalent modification of glassy carbon electrode by Nile blue: Preparation, electrochemistry and electrocatalysis.* Electrochimica Acta, 2010. **55**(24): p. 7246-7253.
46. Yu, S.S.C., Tan, E. S. Q., Jane, R. T., Downard, A. J., *An electrochemical and XPS study of reduction of nitrophenyl films covalently grafted to planar carbon surfaces.* Langmuir, 2007. **23**(22): p. 11074-11082.
47. Jarillo-Herrero, P.S., M. S., *Understanding and controlling the substrate effect on graphene electron-transfer chemistry via reactivity imprint lithography.* Nature Chem. , 2012. **12**(9): p. 724-32.
48. Chen, H.J., Wang, Y.L., Qu, J.Y., & Dong, S.J., *Self-assembled silver nanoparticle monolayer on glassy carbon: an approach to SERS substrate.* Journal of Raman Spectroscopy, 2007. **38**(11): p. 1444-1448.
49. Sinitskii, A., Ayrat Dimiev,David A. Corley, Alexandra A. Fursina, Dmitry V. Kosynkin, and James M. Tour, *Kinetics of Diazonium Functionalization of Chemically Converted Graphene Nanoribbons.* ACS Nano, 2010. **4** (4): p. 1949-1954.
50. Sharma, R., Joon Hyun Baik, Chrisantha J. Perera, and Michael S. Strano, *Anomalously Large Reactivity of Single Graphene Layers and Edges toward Electron Transfer Chemistries.* Nano Lett. , 2010. **10**: p. 398-405.
51. Dumitrescu, L., N.R. Wilson, and J.V. Macpherson, *Functionalizing single-walled carbon nanotube networks: Effect on electrical and electrochemical properties.* Journal of Physical Chemistry C, 2007. **111**(35): p. 12944-12953.
52. Genorio, B., Lu, W., Dimiev, A. M., Zhu, Y., Raji, A. R. O., Novosel, B., Alemany, L. B., Tour, J. M., *In Situ Intercalation Replacement and Selective Functionalization of Graphene Nanoribbon Stacks.* Acs Nano, 2012. **6**(5): p. 4231-4240.
53. Mohanty, N., & Berry, V, *Graphene-Based Single-Bacterium Resolution Biodevice and DNA Transistor: Interfacing Graphene Derivatives with Nanoscale and Microscale Biocomponents.* Nano Lett., 2008. **8**.
54. Kumar, B., Min, K., Bashirzadeh, M., Farimani, A. B., Bae, M. H., Estrada, D., Kim, Y. D., Yasaei, P., Park, Y. D., Pop, E., Aluru, N. R., Salehi-Khojin, A., *The Role of External Defects in Chemical Sensing of Graphene Field-Effect Transistors.* Nano letters, 2013. **13**(5): p. 1962-1968.
55. Camara, N., Tiberj, Antoine, Jouault, Benoit, Caboni, Alessandra, Jabakhanji, Bilal, Mestres, Narcis, Godignon, Philippe, Camassel, Jean, *Current status of self-organized epitaxial graphene ribbons on the C face of 6H-SiC substrates.* Journal of Physics D-Applied Physics, 2010. **43**(37).